Solar Energy 140 (2016) 73–82

Contents lists available at ScienceDirect

Solar Energy

journal homepage: www.elsevier.com/locate/solener

A full thermal model for photovoltaic devices

Olivier Dupré [a,b,*], Rodolphe Vaillon [a,c], Martin A. Green [b]

[a] Univ Lyon, CNRS, INSA-Lyon, Université Claude Bernard Lyon 1, CETHIL UMR5008, F-69621 Villeurbanne, France
[b] Australian Centre for Advanced Photovoltaics (ACAP), School of Photovoltaic and Renewable Energy Engineering, University of New South Wales, Sydney 2052, Australia
[c] W.W. Clyde Visiting Chair, Radiative Energy Transfer Laboratory, Department of Mechanical Engineering, University of Utah, Salt Lake City, UT 84112, USA

ARTICLE INFO

Article history:
Received 24 May 2016
Received in revised form 11 October 2016
Accepted 19 October 2016
Available online 4 November 2016

Keywords:
Thermal modeling
Photovoltaics
Solar cells
Temperature
NOCT
Optimization

ABSTRACT

A full thermal model for photovoltaic devices is presented. It consists of describing the physics of the conversion losses that come with heat dissipation together with giving analytical expressions of the associated heat sources. The consistency of the model is demonstrated by its application to a crystalline silicon solar cell. The modeling is completed by the balance equation which drives the equilibrium temperature of the cell. The impact of considering a full thermal model for designing photovoltaic devices is illustrated with two examples related to solar cells. First, the dependence of the heat source on the applied bias suggests that the Nominal Operating Cell Temperature should be defined at the Maximum Power Point instead of at open circuit and also could be function of representative climate conditions and mounting configurations. Second, a simple combined analysis of the heat source and the dependence of output electrical power with temperature – i.e. temperature coefficient – suggests that taking into consideration a full thermal modeling of solar cells has an impact on choosing the semiconductor material that maximizes the efficiency in real operating conditions.

1. Introduction

The output power of most photovoltaic (PV) devices drops when their temperature increases. This fact is particularly well known for solar cells (Virtuani et al., 2010). Indeed, when predicting the energy yield of solar cell installations, variations of output power with module temperature need to be accounted for, as a function of the local climate (Kurtz et al., 2011) and the mounting configuration. To this end, semi-empirical models giving an estimate of the cell temperature or directly the efficiency were proposed (see reviews in (Skoplaki and Palyvos, 2009a,b)). In order to reduce the efficiency loss due to a rise in temperature, it is possible to act in different ways on the thermal behavior of a PV device (see Fig. 1). The decrease rate of the electrical output power per cell surface area (P_{MPP}, in W m^{-2}) with the cell temperature (T_c), called temperature coefficient (β), has to be as small as possible. It is necessary to go in depth into the physics ruling these coefficients (Dupré et al., 2015) for deriving adequate reduction strategies. Also, the PV device temperature has to be as low as possible. In this case, there are two options. The cell has to be efficiently cooled: it requires the thermal exchange coefficient (h in W m^{-2} K^{-1}) to be high, and the ambient temperature (T_{amb}) and that of the environment with which thermal radiation is exchanged (T_e) to be low. The need for cooling has to be reduced: the heat dissipation within the cell (total heat source per cell surface area, Q in W m^{-2}) should be limited.

In most cases, the incident irradiation spectrum can be measured easily. If the radiation power absorbed in the cell can be calculated (either directly or from the reflected and transmitted powers), then the heat source is found by simply subtracting the electrical output power.[1] The other way for determining the total heat source consists in the calculation of each component contributing to it and the summation of all components. One advantage, usually overlooked, is that this way enables new optimizations that reduce heat dissipation - thus the operating temperature – and in turn provide a larger electrical output in given operating conditions (see for example (Dupré and Vaillon, 2014) for solar cells and (Bernardi et al., 2015) for TPV cells with near-field interactions).

* Corresponding author at: Univ Lyon, CNRS, INSA-Lyon, Université Claude Bernard Lyon 1, CETHIL UMR5008, F-69621 Villeurbanne, France.
E-mail address: olivier.dupre@insa-lyon.fr (O. Dupré).

[1] To be fully exact, emission from the cell due to radiative recombination should be also subtracted, but it is generally negligible for today's PV devices (note that it becomes gradually important as cells' performances get closer to the radiative limit, i.e. certain GaAs solar cells (Green, 2012)). Also, specific photovoltaic converters require somewhat complicated and hence computationally demanding radiative transfer calculations (e.g. thermophotovoltaic (TPV) cells with near-field interactions (Whale and Cravalho, 2002; Francoeur et al., 2011)).

http://dx.doi.org/10.1016/j.solener.2016.10.033
0038-092X/

Nomenclature

Fundamental constants

c	speed of light in vacuum ($\approx 2.99792458 \cdot 10^8$ m s^{-1})
h	Planck constant ($\approx 6.62606957 \cdot 10^{-34}$ J s)
k	Boltzmann constant ($\approx 1.3806505 \cdot 10^{-23}$ J K^{-1})
q	elementary charge ($\approx 1.60217653 \cdot 10^{-19}$ C)
σ	Stefan-Boltzmann constant ($\approx 5.67037321 \cdot 10^{-8}$ W m^{-2} K^{-4})

Latin symbols

E	photon energy (eV)
E_c	conduction band edge (eV)
E_{Fn}	quasi-Fermi level of the electrons
E_g	energy bandgap (eV)
EQE	external quantum efficiency
ERE	external radiative efficiency
f	fraction of photons
h	heat transfer coefficient (W m^{-2} K^{-1})
J	current density (A m^{-2})
J_{max}	maximum current density (A m^{-2})
P	power loss per unit area not being a heat source (W m^{-2})
PFD	photon flux density (m^{-2})
$PFD_{bb(T)}$	photon flux density emitted by a blackbody at temperature T (m^{-2})
Q	component of the heat generated in the device per unit area, heat flux (W m^{-2})
$R(E)$	spectral reflectance of the PV device
R_s	series resistance (Ω)
R_{sh}	shunt resistance (Ω)
$T(E)$	spectral transmittance of the PV device
T_{amb}	ambient temperature
T_e	temperature of the environment with which the device exchanges thermal radiation
V	voltage (V)
V_{max}	maximum voltage (V)

Greek symbols

β	temperature coefficient (ppm K^{-1} or % K^{-1})
Δ	for specifying a current (ΔJ) or a voltage (ΔV) loss with respect to the maximum
$\varepsilon(E)$	spectral emittance of the PV device
Ω	(projected) solid angle
Π	Peltier coefficient (V)

Subscripts

0	in the dark (applies to the current density)
abs	applies to the (projected) solid angle under which the cell absorbs radiation from the source
am	refers to the angle mismatch loss
bb	refers to the case where the illumination (or the cell) radiation is modelled by a blackbody (Planck function)
below E_g	refers to the sub-bandgap loss
c	refers to the cell (temperature only)
Carnot	Carnot fundamental loss
cond, conv, rad	apply to the heat fluxes exchanged by the cell with its surrounding by conduction, convection, radiation
current	for the fraction of photons that participate to the current
ΔJ, ΔV	applies to the heat source components associated to a current loss or a voltage loss
emit	applies to the (projected) solid angle within which the cell emits radiation
ex	for the fraction of photons emitted that exit the cell
ib	for the fraction of photons absorbed through the inter-band process
oc	open circuit
par	for the fraction of photons absorbed through the parasitic processes
s	refers to the Sun (equivalent blackbody temperature only) or series (for resistances)
sc	short circuit

Abbreviations

FCA	free-carrier absorption
MPP	maximum power point
NOCT	nominal operating cell temperature
NRR	non radiative recombination
RR	radiative recombination

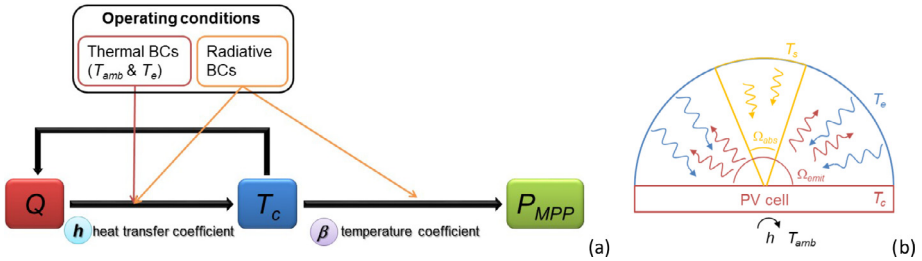

Fig. 1. a. Schematic of the thermal behavior of photovoltaic devices adapted from (Dupré and Vaillon, 2014). Radiative boundary conditions can be simply the incident irradiation spectrum (for solar and solar TPV cells) and/or the radiator radiative properties and temperature (for TPV cells). b. Schematic defining the main parameters for establishing the thermal and radiative boundary conditions. T_s and T_c are respectively the temperature of the source and that of the PV cell. T_{amb} and T_e are respectively the ambient temperature and the temperature of the environment with which the device exchanges thermal radiation.

Determination of the mechanisms contributing to heat dissipation in photovoltaic devices was part of previous articles having different objectives (e.g. interpreting specific experiments (Dramićanin et al., 1995; Breitenstein and Rakotoniaina, 2005) or analyzing the thermal behavior of PV devices (Francoeur et al., 2011; Bernardi et al., 2015)), but to date no comprehensive and fully consistent analytical thermal modeling is available. In this article, a full thermal model for photovoltaic devices is proposed. Each conversion loss mechanism is taken properly into account and an analytical expression of the corresponding heat source is given. The reliability of the resulting total heat source is shown by applying the model to a crystalline silicon (c-Si) solar cell and by checking the overall current density, voltage, and power balances. The thermal analysis is completed by recalling briefly how

to determine the PV device equilibrium temperature. In the subsequent section, benefits of such a full thermal modeling are further demonstrated by introducing a thermal engineering vision of solar cell performances. First, the Nominal Operating Cell Temperature (NOCT) is revisited by considering the variations of the heat source with the applied voltage. Then, a simple performance analysis including the thermal behavior shows that the primary choice of a solar cell semiconductor material depends on the operating conditions.

2. A full thermal model

The building of a full thermal model is based on listing the existing conversion losses and on deriving an analytical expression of the heat source when the loss comes with heat dissipation within the PV device. In order to remain as general as possible, a p-n junction with energy band gap E_g subjected to a known illumination (Photon Flux Density *PFD* as a function of photon energy E) is considered.[2] Each heat source associated to a loss mechanism is calculated for the whole cell per unit cell area ($Q_{mechanism}$ in W m^{-2}), knowing that deriving local expressions of the same source per unit volume (in W m^{-3}) is not a difficult task. Indeed, the existing thermal models solving for thermal diffusion within the cell have led to the conclusion that the resulting temperature difference across the cell is small (Francoeur et al., 2011). Thus the thermal problem consists simply in searching for the temperature of the cell that balances the heat fluxes exchanged by the cell and its surrounding, with the global –i.e. spatially integrated- heat source generated within the cell.

2.1. Conversion losses and heat sources

Following the methodology described elsewhere (Dupré et al., 2015), Fig. 2 depicts the conversion losses in a standard p-n junction. For the sake of completeness, all losses, even those not leading to heat dissipation, are included in the analysis (and will be noted $P_{mechanism}$). This will ultimately allow checking the modeling consistency by calculating the overall power balance for the incident radiation. Power associated to loss mechanisms generating heat dissipation are noted $Q_{mechanism}$. The conversion losses can be conveniently sketched on a dual axis plot (Fig. 3) showing the cumulated incident photon flux density times electrical elementary charge as a function of photon energy and also cell current density as a function of cell voltage (*J-V* characteristic). Each transformation process of the incident radiation power can be identified. The maximum voltage ($V_{\max}$) that can build in the cell is E_g/q (E_g in eV). The maximum current density ($J_{\max}$) corresponds to the case where the cumulated incident photon density with photon energy larger than the band gap is entirely absorbed and contributes to the current, i.e. $J_{\max} = q \int_{E_g}^{\infty} PFD(E)\,dE$. All the losses at any point on the *J-V* characteristic can be split into current (ΔJ) and voltage (ΔV) losses with corresponding powers $J(V)\ \Delta V$ (V) and $\Delta J(V)\ V_{\max}$ (areas on Fig. 3 in the case where the cell operates at the maximum power point, i.e. $V = V_{MPP}$). Throughout the present section, the reader can refer to both Figs. 2 and 3 to identify each loss mechanism and its physical nature.

The reflection loss corresponds to the fraction of the incident photons (depicted on the left in Fig. 2) that is reflected by the device. It can be expressed as:

$$P_{reflection} = \int_0^{\infty} R(E)\ PFD(E)\ E\,dE \tag{1}$$

[2] In the specific case of TPV converters with near-field interaction, it is not possible to do so because evanescent modes add to the propagative modes, but the transcription of the following methodology to that case is straightforward.

where $R(E)$ is the spectral reflectance of the device. Another optical loss is the transmission loss which corresponds to the photons that pass through the cell unabsorbed. The corresponding power loss ($P_{transmission}$) expression is the same as for the reflection loss with the spectral transmittance of the device $T(E)$ in place of the spectral reflectance. For photon energies larger than the bandgap, the corresponding current loss writes:

$$\Delta J_{reflection+transmission} = q \int_{E_g}^{\infty} (R(E) + T(E))\ PFD(E)\,dE \tag{2}$$

with a power loss given by $\Delta J_{reflection+transmission}\ E_g/q$.

The below E_g loss originates from the incident photons that are not reflected and that do not have enough energy to excite an electron across the bandgap. These photons either leave the cell or are absorbed by the lattice atoms or by the free-carriers or by the rear metallization. In the case where the photons are absorbed (not depicted in Fig. 2), their energy is transferred to phonons (either directly for lattice absorption or through a subsequent thermalization process in the case of free-carrier absorption) and they contribute to the heat source:

$$Q_{below\ E_g} = \int_0^{E_g} (1 - R(E) - T(E))\ PFD(E)\ E\,dE \tag{3}$$

Photons with energy larger than the bandgap can also be absorbed by the lattice atoms or by the free-carriers (not depicted in Fig. 2). These absorption mechanisms compete with interband absorption and thus are called parasitic absorption. The corresponding heat source is:

$$Q_{parasitic\ abs.} = \int_{E_g}^{\infty} (1 - R(E) - T(E))\, f_{par}(E)\ PFD(E)\ E\,dE \tag{4}$$

where f_{par} is the fraction of photons absorbed through parasitic processes (lattice and free-carriers).

The thermalization loss relates to the excited electrical carriers which relax some of their energy extremely quickly towards the band edges to reach their thermal equilibrium distribution (in about 10^{-12} s (Würfel, 2009)). The energy in excess of the bandgap is transferred to the phonons and the associated heat source reads:

$$Q_{thermalization} = \int_{E_g}^{\infty} (1 - R(E) - T(E))\, f_{ib}(E)\ PFD(E)\ (E - E_g)\,dE \tag{5}$$

where f_{ib} is the fraction of photons absorbed through the interband process. Note that because the photons that don't leave the cells have to be absorbed eventually, $f_{ib}(E) + f_{par}(E) = 1$.

The emission loss corresponds to the photons emitted by the device resulting from radiative recombination. The associated rate of photon emission depends on bias voltage (V) and can be derived using Rau's reciprocity principle (Rau, 2007; Dupré et al., 2015):

$$emission\_rate(V) = \frac{2\,\Omega_{emit}}{c^2 h^3} \int_0^{\infty} \frac{\overline{EQE}\ E^2}{\exp\left(\frac{E - qV}{kT_c}\right) - 1} dE \tag{6}$$

where c, q, k and h are respectively the light speed in vacuum, the elementary electrical charge, Boltzmann and Planck constants, and Ω_{emit} is the integral over the emission solid angle of the polar angle cosine but it is simply referred to as a solid angle as in (Harder and Würfel, 2003). $\overline{EQE}$ is the external quantum efficiency of the cell appropriately weighted over all angles of incident light (Green, 2012). The corresponding current loss is simply $\Delta J_{emission}(V) = q\ emission\_rate(V)$.

The energy of the emitted photons is approximately equal to the bandgap energy so the power lost through photon emission originally caused by radiative recombination is:

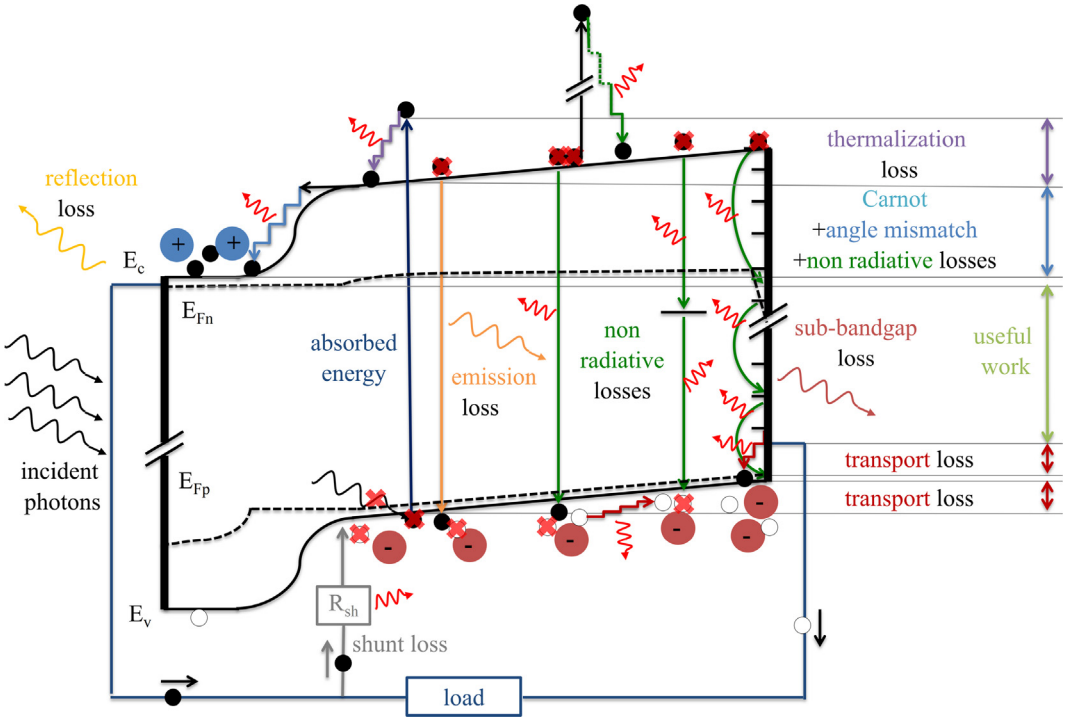

Fig. 2. p-n Junction diagram showing the energy conversion loss processes in a standard single junction PV cell adapted from (Dupré et al., 2015). The large curly arrows represent photons and the small curly arrows represent phonons. As the electrical carriers go down the potential gradients (step arrows), they transfer energy to the phonons. Non radiative recombination, transport and shunt losses also come with energy transfer to the phonons.

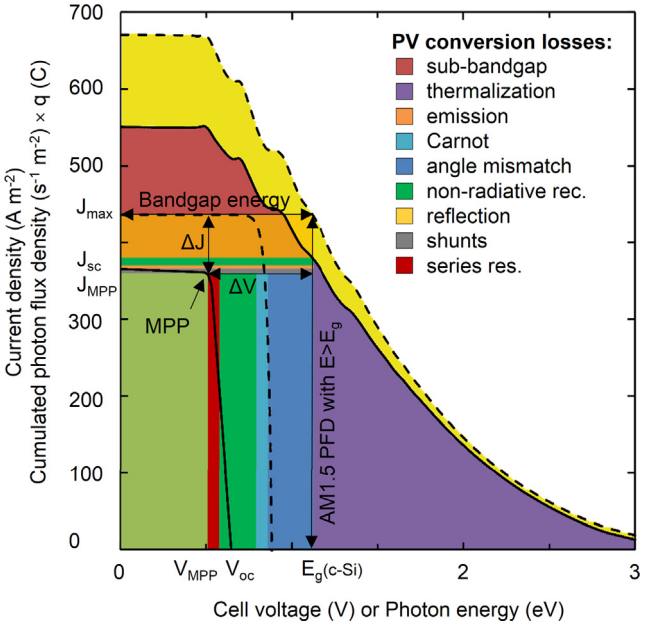

Fig. 3. Dual axis representation of: the AM1.5 cumulated photon flux density times electrical elementary charge (dashed line: potential maximum current from the incident photons; full line: from the absorbed photons) as a function of photon energy; of current density as a function of voltage, for a c-Si solar cell with a planar surface without anti-reflection coating adapted from (Dupré et al., 2015). The different conversion losses are identified by the color code shown in the legend.

$$P_{emission}(V) = emission\_rate(V)\,E_g = \Delta J_{emission}(V)\,\frac{E_g}{q} = E_g\,\frac{2\,\Omega_{emit}}{c^2\,h^3}\int_{Eg}^{\infty}\frac{\overline{EQE}\,E^2}{\exp\left(\frac{E-qV}{kT_c}\right)-1}\,dE \quad (7)$$

The radiative recombination rate can be much larger than the external photon emission rate given by Eq. (6). Typically, when light trapping is efficient, most of the photons emitted via radiative recombination are reabsorbed (via either interband or parasitic processes) within the cell and only a fraction of these photons is emitted outside the cell. An illustration can be found in (Richter et al., 2013) where the spectrally resolved probabilities of these different events have been calculated for a 200-μm-thick undoped silicon wafer at 25 °C.

Parasitic absorptions of the photons emitted via radiative recombination are the cause of heat dissipation:

$$Q_{RR-parasitic\ abs.}(V) = f_{par}\,RR(V) = f_{par}\,(P_{emission}(V)/f_{ex}) \quad (8)$$

where $RR(V)$ is the total energy lost by radiative recombination, f_{par} is the fraction (or probability) of that energy that is absorbed by parasitic processes and f_{ex} is the probability that a photon emitted in the cell exits from it. Logically, the energy corresponding to radiative recombination ($RR(V)$) is equal to the energy emitted out of the cell ($P_{emission}(V)$) divided by the fraction f_{ex}. Note that parasitic absorption is generally dominated by free-carrier absorption (FCA) on this spectral range, especially when the excess carrier density is high.

The photons that are reabsorbed in an interband process generate excited carriers that will either participate to the current or recombine either via a radiative or a non-radiative process. In the latter case, they will generate a heat source:

$$Q_{NRR-RR}(V) = f_{NRR}\,RR(V) = f_{NRR}\,(P_{emission}(V)/f_{ex}) \quad (9)$$

where f_{NRR} is the fraction of the photons emitted via radiative recombination that generates another carrier that recombines non-radiatively (subscript *NRR* added).

In summary, a photon emitted via radiative recombination can either leave the cell (f_{ex}), be absorbed by a parasitic process (f_{par}), be reabsorbed (interband process) and generate a carrier that recombines non-radiatively (f_{NRR}), be reabsorbed (interband process) and generate a carrier that participates to the current ($f_{current}$). From conservation principles, $f_{par} + f_{NRR} + f_{ex} + f_{current} = 1$.

The Carnot loss described in (Landsberg and Badescu, 2000; Hirst and Ekins-Daukes, 2011), is the minimum energy required to separate the photogenerated charges. Indeed, a solar cell converts the thermal energy of the Sun and is thus fundamentally limited by the Carnot efficiency that involves its temperature and that of the Sun. The Carnot loss shown in Fig. 2 can also be seen as the voltage drop associated with the minimum recombination rate which equals the rate of radiative emission in the solid angle into which the cell absorbs the solar photons. Within the assumptions made in (Hirst and Ekins-Daukes, 2011) (radiative limit, Boltzmann approximation of the generalized Planck function, ...), it is possible to derive the voltage drop (ΔV_{MPP}) at maximum power point (MPP) for a radiation source (Sun or hot body) modelled by a blackbody at source temperature (T_s) as:

$$\Delta V_{MPP-Carnot-bb} = \frac{E_g}{q}\frac{T_c}{T_s} \tag{10}$$

where notation "*bb*" indicates that the expression is derived assuming the radiative exchanges between blackbodies. The corresponding heat source is given by:

$$Q_{Carnot-bb}(V_{MPP}) = J_{MPP}\Delta V_{MPP-Carnot-bb} = J_{MPP}\frac{E_g}{q}\frac{T_c}{T_s} \tag{11}$$

The next loss, the so-called angle mismatch loss, originates from the fact that the cell usually emits radiation in a solid angle larger than the solid angle of absorption of the source photons (e.g. for the standard non-concentrated solar cells), the minimal - radiative - recombination rate is larger than in the case described above. This implies that the generation/recombination balance is a function of the solid angle ratio between emission and absorption. In the radiative limit and with the same assumptions introduced previously, the voltage drop at the maximum power point is approximately equal to (Hirst and Ekins-Daukes, 2011):

$$\Delta V_{MPP-am-bb} \approx \frac{kT_c}{q}\ln\left(\frac{\Omega_{emit}}{\Omega_{abs}}\right) \tag{12}$$

The heat generation corresponding to the voltage reduction associated to the angle mismatch is equal to:

$$Q_{am-bb}(V_{MPP}) = J_{MPP}\Delta V_{MPP-am-bb} = J_{MPP}\frac{kT_c}{q}\ln\left(\frac{\Omega_{emit}}{\Omega_{abs}}\right) \tag{13}$$

Non-radiative recombination (NRR) losses arise in real PV cells in addition to the radiative recombination loss (see Fig. 2 that depicts the different mechanisms: Auger, Shockley-Read-Hall, ...). A consequence is that the excess energy ($\approx E_g$) of the electron that goes back to the valence band is transferred to the phonons. NRR recombinations reduce the current that can be extracted from the cell and limit the voltage that can build in the cell. The concept of External Radiative Efficiency (ERE), which corresponds to the fraction of recombination events that results in the emission of a photon from the device (Green, 2012), can be used to quantify the non-radiative recombination losses. Thus the rate of non-radiative recombination is simply $NRR\_rate(V) = emission\_rate(V)(1/ERE - 1)$. The heat generation resulting from current losses caused by NRR events is:

$$\begin{aligned} Q_{NRR-\Delta J}(V) &= NRR\_rate(V)\,E_g = \Delta J_{NRR}(V)\,\frac{E_g}{q} \\ &= E_g\left(\frac{1}{ERE} - 1\right)\frac{2\Omega_{emit}}{c^2h^3}\int_{E_g}^{\infty}\frac{\overline{EQE}\,E^2}{\exp\left(\frac{E-qV}{kT_c}\right)-1}\,dE \end{aligned} \tag{14}$$

where subscript ΔJ indicates that this NRR loss corresponds to a current loss and where the minus one term in brackets stands for the subtraction of the power leaving the cell due to radiative recombination ($P_{emission}$) since it does not contribute to the heat source.

By applying the usual assumptions, when the incident radiation can be modelled by a blackbody at temperature T_s and following (Dupré et al., 2015), the subsequent approximation can be derived for the voltage drop at the maximum power point (Dupré, 2015):

$$\Delta V_{MPP-NRR-bb} \approx \frac{kT_c}{q}\ln\left(\frac{1}{ERE_{MPP}}\right) \tag{15}$$

The corresponding heat source at MPP reads:

$$Q_{NRR-\Delta V-bb}(V_{MPP}) = J_{MPP}\,\Delta V_{MPP-NRR-bb} = J_{MPP}\frac{kT_c}{q}\ln\left(\frac{1}{ERE_{MPP}}\right) \tag{16}$$

Transport loss is inevitable in real solar cells. Along their paths, carriers lose some of their potential energy through collisions with the lattice atoms or other carriers (illustrated in Fig. 2). This corresponds to a potential loss proportional to the cell series resistance (R_s) and the flow of carriers ($\Delta V_{transport}(V) = R_s J(V)$). The cell series resistance can also include local resistances at the contacts. The corresponding energy loss is also known as Joule heating (RI^2):

$$Q_{transport}(V) = J(V)\,\Delta V_{transport}(V) = R_s J^2(V) \tag{17}$$

Considering the addition of all voltage losses (Carnot, angle mismatch, non-radiative recombination, transport), the operating voltage can be written in the compact form $V = V_{\max} - \Delta V$. The heat source associated to the voltage drop is simply:

$$Q_{\Delta V}(V) = J(V)\,\Delta V = J(V)\,(V_{\max} - V) \tag{18}$$

At the maximum power point:

$$\begin{aligned} &Q_{\Delta V}(V_{MPP}) = J(V_{MPP})(V_{\max} - V_{MPP}) = J_{MPP}\Delta V_{MPP} \\ &= J_{MPP}(\Delta V_{MPP-Carnot} + \Delta V_{MPP-am} + \Delta V_{MPP-NRR} + \Delta V_{transport}) \end{aligned} \tag{19}$$

If the radiative exchanges can be modelled as that of blackbodies, then the voltage at maximum power point has an analytical expression:

$$\begin{aligned} V_{MPP} &= V_{\max} - \Delta V_{MPP-Carnot-bb} - \Delta V_{MPP-am-bb} - \Delta V_{MPP-NRR-bb} \\ &\quad - \Delta V_{MPP-transport} \\ &= \frac{E_g}{q}\left(1 - \frac{T_c}{T_s}\right) - \frac{kT_c}{q}\ln\left(\frac{\Omega_{emit}}{\Omega_{abs}}\right) - \frac{kT_c}{q}\ln\left(\frac{1}{ERE_{MPP}}\right) \\ &\quad - R_s J_{MPP} \end{aligned} \tag{20}$$

Then, the heat source associated to the voltage drop at maximum power point can be written:

$$\begin{aligned} Q_{MPP-\Delta V-bb} &= J_{MPP}\Delta V_{MPP} \\ &= J_{MPP}\left(\frac{E_g}{q}\frac{T_c}{T_s} + \frac{kT_c}{q}\ln\left(\frac{\Omega_{emit}}{\Omega_{abs}}\right) + \frac{kT_c}{q}\ln\left(\frac{1}{ERE_{MPP}}\right) + R_s J_{MPP}\right) \end{aligned} \tag{21}$$

For an arbitrary irradiation ($PFD(E)$), the *J-V* characteristics can be calculated numerically and J_{MPP} and V_{MPP} easily extracted.[3] Consequently, the heat source due to voltages drops is deduced from Eq. (19) and in particular from Eq. (20) at the maximum power point.

It is worth noticing that the voltage loss is mostly taking place at the p-n junction and at the peripheral regions. The carriers that circulate through the circuit lose a fraction of their potential energy at the interfaces of the selective membranes (the p-n

[3] When considering a spectral radiative emissions different from that of blackbodies (the reference AM1.5 spectrum for example), it is not possible to obtain simple analytical expressions for the different voltage losses. However, these can be estimated numerically by calculating the maximum power point of the cell assuming different values for J_0, the total recombination rate at $V = 0$. Setting its value to that of the minimum photon emission rate from the cell, when the cell's radiation absorption and emission channels are matched, one obtains V_{MPP} in the Carnot limit. The angle mismatch and the non-radiative recombination losses can be calculated by setting J_0 to the actual photon emission rate multiplied by one and by $1/ERE$ respectively.

junction in the example illustrated in Fig. 2). For example, when going from the conduction band of the P-side to that of the N-side, the electrons accelerate by losing some of their electric potential. Then, they quickly slow down - to their initial average thermal velocity - through collisions with the lattice atoms. This thermalization resulting in heat generation ($Q_{\Delta V} = J(V)\Delta V$), which occurs mostly at the p-n junction, can be assimilated to Peltier heating (Breitenstein and Rakotoniaina, 2005). Indeed, the voltage drop at the junction ($\Delta V_{junction}$) also corresponds to the difference of the Peltier coefficients between the P and the N doped regions ($\Pi_P - \Pi_N$). Following (Pipe et al., 2002), a material's Peltier coefficient is related to the average energy (with respect to the Fermi energy) transported by its electrical carriers ($\bar{E}_{tr}$) through $|\Pi| = \bar{E}_{tr}/q$. The average energy of electrons in the conduction band with respect to the quasi-Fermi energy is (Kittel, 1996): $\bar{E}_{tr} = (E_c - E_{Fn} + 3/2kT_c)$, where E_c is the conduction band edge energy and E_{Fn} is the quasi-Fermi level of the electrons. It results that $(\Pi_P - \Pi_N) = (E_c(P) - E_c(N))/q = \Delta V_{junction}$, and as expected, the Peltier heating source term at the junction reads: $Q_{Peltier} = J(V)(\Pi_P - \Pi_N) = J(V)\Delta V_{junction}$. The same analysis holds at any place in the cell with sharp spatial variations of the band edges.

Shunt loss comes from shunt paths that can be assimilated to recombination paths as they also result in the de-excitation of electrons (see Fig. 2). The shunt resistance (R_{sh}) of a solar cell characterizes the "leakage across the p-n junction around the edge of the cell and within the cell in the presence of crystal defects and precipitates of foreign impurities in the junction region" (Green, 1982). The heat source associated to shunt paths is:

$$Q_{shunt}(V) = shunt\_rate(V)\, E_g = \Delta J_{shunt}(V)\, \frac{E_g}{q} \tag{22}$$

The shunt loss rate can be extracted from the calculated *J-V* characteristics and using a single diode model:

$$shunt\_rate(V) = \frac{V + J(V)\, R_s}{R_{sh}} \tag{23}$$

This equation indicates that losses via shunt paths increase linearly with bias/voltage, contrary to most recombination rates which increase exponentially with voltage. This explains why, for common shunt resistance values, shunt paths effectively reduce J_{sc} and J_{MPP} but don't impact V_{MPP} or V_{oc}.

Finally, the electrical carriers that did not recombine on their way and did not take shunt paths (J) flow through the load where they dissipate the excess potential energy they have (V). This result in an electrical power $P_{elec.}(V) = J(V)\, V$ (at the maximum power point: $P_{MPP} = J_{MPP}V_{MPP}$).

The total heat source generated within the cell is a function of the operating point on the *J-V* characteristics and is finally given, in a compact form, by:

$$\begin{aligned} Q(V) = {} & Q_{below\ E_g} + Q_{parasitic\ abs.} + Q_{thermalization} \\ & + Q_{RR-parasitic\ abs.}(V) + Q_{RR-NRR}(V) + Q_{NRR-\Delta J}(V) \\ & + Q_{\Delta V}(V) + Q_{shunt}(V) \end{aligned} \tag{24}$$

The first three terms (given by Eqs. (3), (4) and (5)) neither depend on J nor on V, while the remaining ones (given by Eqs. (8) and (9) with (7), (14), (18) - (19) at MPP -, and (22) with (23)) do depend on the operating point on the *J-V* characteristics. This means that the heat dissipation is different when considering the short circuit, open circuit or maximum power points (see Section 3.1. for a discussion about the impact of this statement).

2.2. Application to a c-Si solar cell

For illustration, the previous heat source model is applied to the case of a crystalline silicon (c-Si) solar cell (E_g = 1.12 eV at 25 °C) under an AM1.5 solar illumination (incident power density: 1000 W m^{-2}). For the sake of simplicity, the front surface is assumed perfectly smooth without any anti-reflection coating. An ideal interband absorption is assumed (f_{ib} = 1 for $E \geqslant E_g$), i.e. without any parasitic absorption (f_{par} = 0). Any photon emitted via radiative recombination leaves the cell (f_{ex} = 1 and $f_{NRR} = f_{current}$ = 0)). The maximum of the current density – voltage product (JV) is determined numerically using the current density:

$$\begin{aligned} J(V) &= J_{sc,\max} - J_0 \exp\left(\frac{q(V + JR_s)}{kT_c}\right) - \frac{V + JR_s}{R_{sh}} \\ &= q\int_0^{\infty} (1 - R(E) - T(E))\, f_{ib}(E)\, PFD(E)\, dE - \frac{1}{ERE} J_{0,rad} \\ &\quad \times \exp\left(\frac{q(V + JR_s)}{kT_c}\right) - \frac{V + JR_s}{R_{sh}} \end{aligned} \tag{25}$$

where $J_{0,rad} = q\ emission\_rate(V)$ is the current loss associated to radiative emission. The parameters chosen for the calculations are: T_c = 25 °C (298.15 K), R_s = 1.1 Ω cm^2, R_{sh} = 240 Ω cm^2, $ERE = 10^{-5}$, $\Omega_{emit} = \pi$ and $\Omega_{abs} = \Omega_{emit}/46{,}200$ (the solid angle of the Sun from Earth without concentration).

Table 1 displays the current density, voltage, and power density losses resulting from the application of the model described in Section 2.1 and calculated at the maximum power point. In the example, the ERE is too small to lead to a significant emission due to radiative recombination. "Thermalization" and "below Eg" losses are by far the largest contributors to the losses (42.4%) and to the heat source (61.1%). Other fundamental voltage drops (separation losses) such as "Carnot" and "angle mismatch" are contributing up to 11.3% to the losses (13.3% of the heat source). In this configuration, the NRR losses participate to a similar extent to the losses (12%) and to the heat source (13.9%). It is worth noticing that the voltage drops calculated using the analytical expressions that consider that the Sun can be modelled by a blackbody source (in parenthesis in Table 1) are not very different from those numerically calculated using the AM1.5 spectrum. The calculated balances (maximum current density minus the current drops, maximum voltage minus the voltage drops, and incident radiation power minus all loss and electrical output powers) demonstrate that the modeling is fully consistent. These data have been calculated at the maximum power point. Results would be quite different for other operating points (at open circuit or short circuit for example). This will be discussed in depth in Section 3.1.

2.3. Equilibrium temperature

Once the heat source is determined, the temperature of the cell results from a balance between this heat source and the heat lost to the cell's environment. There are three channels of heat exchange: conductive, convective and radiative. Conductive and convective heat transfer can be modelled simply:

$$Q_{cond+conv} = h\,(T_c - T_{amb}) \tag{26}$$

where T_c and T_{amb} are the temperature of the cell and the ambient and h is a global heat transfer coefficient. It is worth noticing that these heat transfer mechanisms increase linearly with the difference between the cell temperature and that of the ambient. Far-field radiative heat transfer has a different dependence on the cell temperature. In the case of gray emission and absorption, it depends on the difference between the cell temperature to the fourth power and the environment temperature to the fourth power:

Table 1
Heat source model applied to a c-Si solar cell (input parameters described in the text) at the maximum power point (J_{MPP}, V_{MPP}): current density, voltage and power density losses and heat sources. The voltage losses in parentheses on lines (f), (g) and (h) are calculated analytically with Sun's radiation spectrum defined by a blackbody at T_s = 5800 K.

		units→	mA cm^{-2}	V	W m^{-2}	%	%
			max short circuit current $J_{sc,max}$	max open circuit voltage	Incident power		
	(a)	maximum (or base)→	43.6	1.124	1000	100	100
		loss name↓	current density loss ΔJ	voltage loss ΔV	power density	of (a)	of (a)-(b)
incident radiation	(b)	reflection	5.7	N/A	148.0	14.8	N/A
absorbed radiation	(c)	emission	0	N/A	0	0	0
heat source	(d)	below Eg	N/A	N/A	141.6	14.2	16.6
	(e)	thermalization	N/A	N/A	282.0	28.2	33.1
	(f)	Carnot	N/A	0.066 (0.058)	22.4	2.2	2.6
	(g)	angle mismatch	N/A	0.269 (0.276)	91.1	9.1	10.7
	(h)	NRR ΔV	N/A	0.285 (0.296)	96.5	9.7	11.3
	(i)	NRR ΔJ	2.0	N/A	22.5	2.3	2.6
	(j)	transport	N/A	0.037	13.8	1.4	1.6
	(k)	shunt	2.1	N/A	23.6	2.4	2.8
	(l)	electrical	J_{MPP} = 33.9	V_{MPP} = 0.467	158.3	15.8	18.6
		balance (a)-(b)-(c)-(d)-(e)-(f)-(g)-(h)-(i)-(j)-(k)-(l)	-0.1	0	0.2	0	0
		heat source (d)+(e)+(f)+(g)+(h)+(i)+(j)+(k)			693.5	69.3	81.4

$$Q_{rad} = \varepsilon \sigma (T_c^4 - T_e^4) \tag{27}$$

where ε is the cell total emittance, σ is the Stefan-Boltzmann constant and T_e the temperature of the medium with which thermal radiation is exchanged. More generally:

$$Q_{rad} = \int_0^\infty \varepsilon(E)\, E\, (PFD_{bb(T_c)}(E) - PFD_{bb(T_e)}(E))dE \tag{28}$$

where $PFD_{bb(T)}$ is the photon flux density emitted by a blackbody at temperature T. In cases with near-field interactions, fluctuational electrodynamics (Mulet et al., 2002) and numerical methods such as the scattering matrix technique for layered media (Francoeur et al., 2009) have to be implemented.

The overall power balance of the cell writes:

$$Q(V) = Q_{cond+conv} + Q_{rad} \tag{29}$$

where $Q(V)$ is given by Eq. (24). The heat removal from a photovoltaic device depends on the heat transfer coefficients, the net thermal radiation exchanged with the environment, the ambient and environment temperatures, and that of the cell itself. For a specific system in a given configuration, these parameters are fixed and the equilibrium cell temperature depends on the heat generation terms described above as illustrated in the schematic of Fig. 1. The heat source being a function of the cell temperature, it follows that the operating temperature and thus the operating efficiency of a PV cell have to be calculated iteratively.

The complete thermal model described previously is of importance for making predictions of the operating temperature of a photovoltaic device as a function of the cell design parameters and the operating conditions (local climate for solar cells, thermal radiation source for TPV devices, and mounting configuration). The next section gives two simple examples that illustrate a thermal engineering vision for improving solar cell performances (and by extension, other photovoltaic devices).

3. A thermal engineering vision of solar cell performances

3.1. Dependence of the heat source on the bias: revisiting the NOCT

Some of the heat source terms described previously have bias dependences. This implies that the heat source and thus the operating temperature of a photovoltaic device depend upon the applied bias. In the following discussion, for the sake of simplicity, the heat sources associated to the thermalization of photogenerated carriers and the heat source due to parasitic absorption of photons with $E < E_g$ will not be considered.

In short-circuit condition ($V = V_{sc} = 0$), most of the excited carriers do not recombine. Through the cell and the load, $J = J_{sc} \approx J_{ph}$, where J_{ph} is the photogenerated current density. Since $V = 0$, the electrical power output is null. All of the power absorbed by the carriers (from the incident solar photons) is dissipated in Peltier heating at the p-n junction and in Joule heating trough the cell. To be exact, there is a fraction of the energy carried by the photogenerated electrical carriers that is not dissipated into heat but that is emitted out of the cell via radiative recombination processes. However, this fraction is negligible in short-circuit even in the radiative limit (because $V = 0$, see Eq. (7)).

In open-circuit condition ($V = V_{oc}$ and $J = 0$), the voltage is such that the recombination rate balances the generation rate. Thus there isn't any current flowing through the cell and the load, and the electrical power output is null. All of the energy carried by the photogenerated carriers is lost via the different recombination processes, resulting in heat generation except for radiative recombination that can lead to photon emission. If the radiative recombi-

nation rate leading to photon emission out of the cell is negligible compared to the non-radiative recombination rate ($ERE < 10^{-3}$), the heat source corresponds to all of the absorbed solar energy (for $E > E_g$, with the thermalization power removed) like in the short-circuit configuration. However, when the cell radiative quality is high enough ($ERE > 10^{-3}$), the heat source can be significantly lower than the absorbed solar energy because a significant fraction of the power is radiatively emitted. In the extreme case (the radiative limit: $ERE = 1$), in open-circuit, all of the absorbed and non-thermalized power is eventually reemitted so the heat source come only from thermalization and eventually parasitic absorption.

The heat generation of utmost importance is that at the maximum power point ($V = V_{MPP}$). In this configuration, some of the absorbed energy is converted into electricity, thus the heat source is smaller than in open and short-circuit conditions. In the c-Si cell example described in Section 2.2, the heat source at MPP is 18.6% lower than in short circuit and open circuit.

This means that correlatively the operating temperature of a cell is also lower at MPP than in open circuit. This observation suggests revisiting the definition of the Nominal Operating Cell Temperature (NOCT). NOCT is defined as the temperature reached by the open-circuited cells in a module mounted on an open-rack with a wind velocity of 1 m s^{-1}, an ambient air temperature of 20 °C and under a 800 W m^{-2} illumination (Ross and Gonzalez, 1980). These conditions have been chosen so that the annual energy produced by a module is well approximated by its efficiency at NOCT, times the average irradiance incident on the module (in kWh/year) at the location of interest (Ross and Smokler, 1986). However, it is interesting to notice in (Ross and Gonzalez, 1980) that the locations used to define these conditions (Albuquerque, Omaha, Miami) are not representative of all the climates/operating conditions that can be found worldwide. Thus, the NOCT is simply an indicator of the quality of the thermal design of the module (how efficiently it evacuates the heat it generates). From the argument above, it is suggested here that it could be interesting to define the NOCT as the temperature reached by a module at its maximum power point rather than in open-circuit (still in a given set of outdoor conditions) (Koehl et al., 2011; Dupré, 2015). This would include the impact of the conversion efficiency of the device in the value of the NOCT. Thus the NOCT would correspond more closely to the temperature reached by the module in "normal" operating conditions since PV modules operate at MPP. Another suggestion is to define several NOCTs for different sets of outdoor conditions (ambient temperature, illumination, wind speed, ...) representative of specific climates and for different mounting configurations. This would stimulate the creation of specific designs of PV modules that would take into account specific average operating conditions.

3.2. Optimum solar cell as a function of operating conditions

This section aims at showing that the optimum bandgap for a solar cell – which is mainly set by the choice of a semiconductor material – depends on the thermal and radiative operating conditions. For simplicity, it is assumed that all of the useful photons ($E \geqslant E_g$) are absorbed and excite an electrical carrier across the bandgap (no optical losses) and all of the photons with less energy than the bandgap are reflected (the "below E_g" loss does not contribute to the heat source). The incident power is thus converted into heat or electrical power except for the terms "below E_g" and "emission". Fig. 4 shows the distributions of the incident solar energy in the radiative limit calculated for a Sun radiation spectrum modelled by a blackbody at 5800 K and assuming two different values for the cell ERE ($ERE = 1$ in the radiative limit: Fig. 4a and $ERE = 10^{-5}$ for a recent commercial cell: Fig. 4b). The different losses within the area bounded by the bold line are those that generate heat in the cell. When $ERE = 1$, the heat source gets smaller for larger bandgap cells, mainly because of the decrease of the "thermalization" power. The additional loss terms in Fig. 4b are due to the non-radiative recombinations. They also decrease with increasing bandgap. The dotted lines correspond to the temperature coefficient of efficiency, calculated numerically at MPP using the modeling described in (Dupré et al., 2015).

Both the heat source and the temperature sensitivity of the cell efficiency decrease with increasing bandgap. These combined behaviors have an impact on the efficiency expected in real operating conditions. Indeed, larger heat sources lead to larger operating temperatures which reduce the conversion efficiencies according to the temperature coefficients. Fig. 5 shows the operating temperature and the resulting efficiency in a given operating condition ($h = 10$ W m^{-2} K^{-1}, $T_{amb} = 25$ °C, thermal radiation exchanges neglected). The operating temperature is calculated iteratively from Eq. (33) and the maximum efficiency (η_{max}) derive from

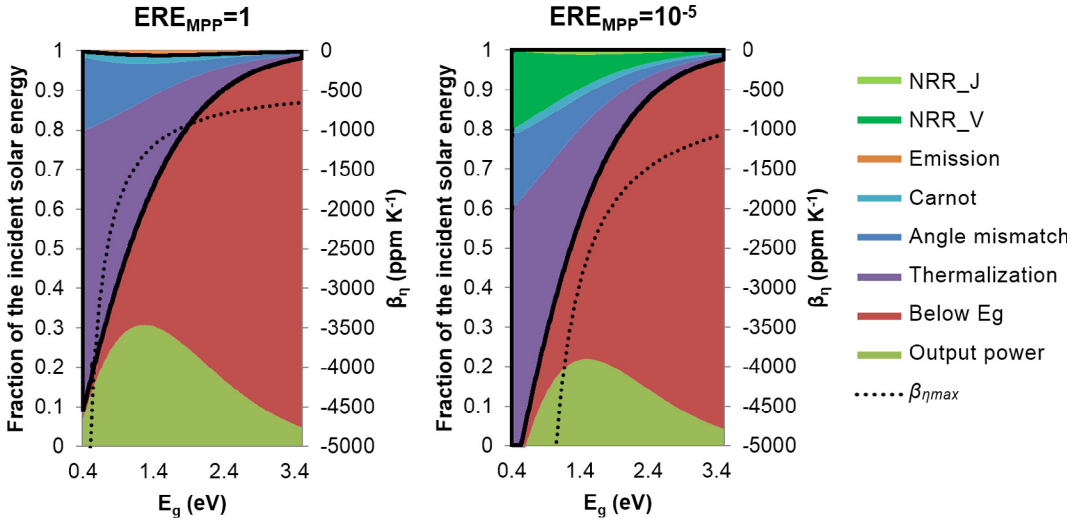

Fig. 4. Distribution of the incident solar radiation at the maximum power point at 300 K as a function of bandgap energy under one Sun illumination: a. in the radiative limit, b. considering an external radiative efficiency equal to 10^{-5}. The dotted line corresponds to the temperature coefficient calculated as a function of bandgap (details given in (Dupré et al., 2015)). The legend on the right describes the color code of the losses on both graphs. Figure from (Dupré, 2015). (For interpretation of the references to colour in this figure legend, the reader is referred to the web version of this article).

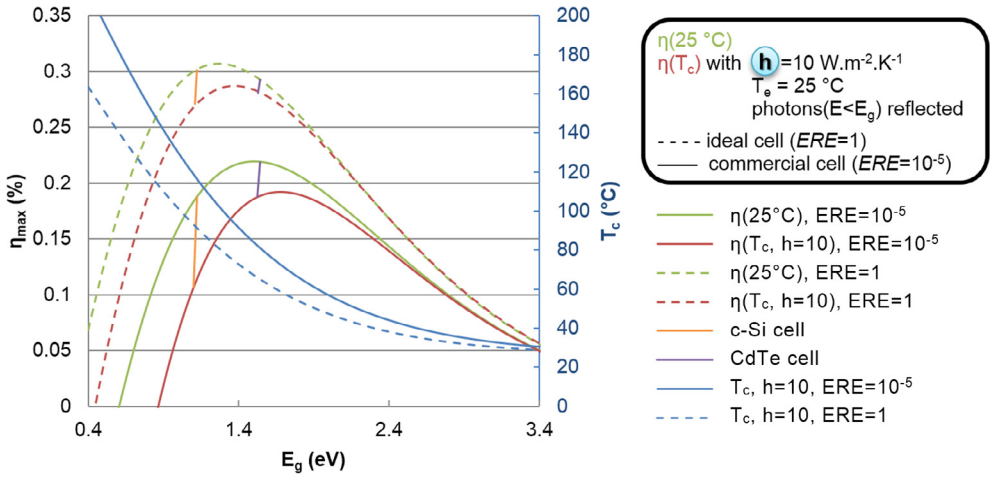

Fig. 5. Illustration of the impact of the bandgap on cell operating temperature and efficiency for an ideal cell (dotted lines) and a commercial cell (full lines). The operating temperature is plotted in blue and is derived from the heat sources depicted in Fig. 4 with $h = 10\ W\ m^{-2}\ K^{-1}$. The efficiencies corresponding to these operating temperatures are plotted in red while the efficiencies assuming that the cell operates at 25 °C are plotted in green. The efficiencies of a c-Si (orange) and a CdTe (purple) cells are shown in the different configurations. Figure from (Dupré, 2015). (For interpretation of the references to colour in this figure legend, the reader is referred to the web version of this article).

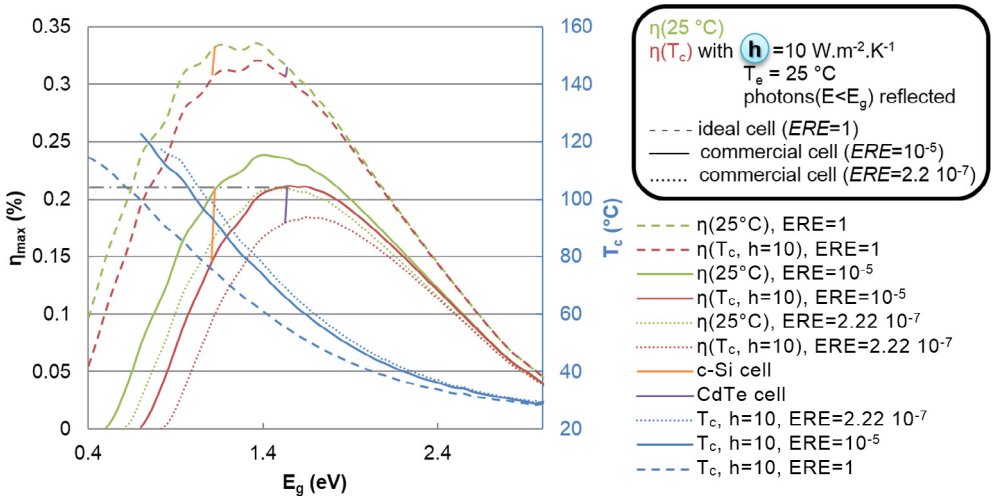

Fig. 6. Illustration of the impact of the bandgap on cell operating temperature and efficiency for an ideal cell (dotted lines), a cell with $ERE = 10^{-5}$ (full lines) and a cell with $ERE = 2.22 \cdot 10^{-7}$ (dotted lines) for an AM1.5 photon flux density. The operating temperatures are plotted in blue and are derived from the heat sources (Section 2) and a heat transfer coefficient $h = 10\ W\ m^{-2}\ K^{-1}$. The efficiencies corresponding to these operating temperatures are plotted in red while the efficiencies assuming that the cell operates at 25 °C are plotted in green. Figure from (Dupré, 2015). (For interpretation of the references to colour in this figure legend, the reader is referred to the web version of this article).

$\eta_{max}(T_c) = \eta_{max}(25\ °C) + 10^{-6}\beta_{\eta max}(T_c - 25\ °C)\ \eta_{max}(25\ °C)$ using the temperature coefficient from Fig. 4. In Fig. 5, dashed lines and full lines correspond to the radiative limit case ($ERE = 1$) and a commercial cell case ($ERE = 10^{-5}$). The efficiencies for the calculated operating cell temperatures are plotted in red and the efficiencies assuming that the cell temperature is equal to 25 °C are plotted in green. As expected, the operating temperature follows the same trend as the heat source (depicted in Fig. 4). Fig. 5 shows that the bandgap that leads to the maximum conversion efficiency is different from that at 25 °C if the thermal operating conditions are taken into account. Of course, this shift depends on the thermal boundary conditions. If the heat transfer coefficient is large enough, the heat generated in the cell does not bring the cell operating temperature above that of the ambient. In this case, there is no interest in reducing the heat generated in the device. However, in the field, PV modules operating temperatures rise significantly above ambient. Thus, their efficiencies could be enhanced by reducing the heat source.

In Fig. 4b, when $ERE = 10^{-5}$, the additional losses both increase the heat source and increase (make worse) the temperature sensitivity of PV cell losses (compared to the radiative limit configuration, $ERE = 1$, depicted in Fig. 4a). This is why considering the cell thermal operating conditions has a larger impact when $ERE = 10^{-5}$ (full lines in Fig. 5) than in the radiative limit (dashed lines, $ERE = 1$). This means that it is especially important to consider the thermal behavior of PV modules with poor conversion efficiencies.

Fig. 5 also depicts the efficiencies corresponding to the bandgaps of c-Si and CdTe in the different scenarios presented above. It illustrates that while these two materials have similar efficiencies in the Shockley-Queisser limit (which corresponds to the green dashed line), their thermal behaviors are quite different. These different thermal behaviors result in an advantage when considering the operating conditions for CdTe (because it has a larger bandgap than c-Si). To enable a fair comparison, calculations were made with two different EREs that correspond to similar

efficiencies at 25 °C for c-Si and CdTe cells. The results, assuming a 1000 W m^{-2} AM1.5 photon flux density, were calculated numerically using the modeling described in Section 2 and are illustrated in Fig. 6. In these conditions ($ERE = 10^{-5}$ and $2.2 \cdot 10^{-7}$ respectively), the c-Si cell operates at a temperature of 94 °C and an efficiency of 14.5% while the CdTe cell operates at a temperature of 69 °C and an efficiency of 17.9%. This calculation explains the advantageous energy yield of modules made from CdTe cells. This analysis also shows that improving module efficiencies result in improved energy yield in the field through the reduction of heat sources and of the temperature coefficients.

4. Conclusion

In this article, it has been shown that modeling the thermal behavior of photovoltaic devices enables to optimize their design as a function of their specific operating conditions. The device temperature is driven by the heat generation and by the conductive, convective and thermal radiative exchanges with the environment. The conversion efficiency is driven by the device temperature via the temperature coefficient which depends upon certain design parameters. For these reasons, a full thermal modeling is of utmost importance. The derivation of analytical expressions of all the heat sources in a PV device makes it possible to undertake thermal optimizations of PV devices. For example, the bias dependence of the heat source call for a modification of the definition of the Nominal Operating Cell Temperature. Also, it has been shown that the optimal choice of a semiconductor material for a solar cell depends on its thermal behavior and on its operating conditions. The full thermal model proposed here enables the optimization of any kind of PV devices (e.g. silicon solar cells (Dupré and Vaillon, 2014), TPV (Bauer, 2013), near-field TPV (Bernardi et al., 2015), solar TPV (Swanson, 1979) and thermophotonics (Harder and Green, 2003) devices) that take into account their operating conditions.

Acknowledgements

ACAP is supported by the Australian Government through the Australian Renewable Energy Agency (ARENA).

References

Bauer, T., 2013. Thermophotovoltaics Basic Principles and Critical Aspects of System Design. Springer, Berlin, Berlin.
Bernardi, M.P., Dupré, O., Blandre, E., et al., 2015. Impacts of propagating, frustrated and surface modes on radiative, electrical and thermal losses in nanoscale-gap thermophotovoltaic power generators. Sci. Rep. 5, 11626. http://dx.doi.org/10.1038/srep11626.
Breitenstein, O., Rakotoniaina, J.P., 2005. Electrothermal simulation of a defect in a solar cell. J. Appl. Phys. 97, 74905. http://dx.doi.org/10.1063/1.1866474.
Dramićanin, M.D., Nikolić, P.M., Ristovski, Z.D., et al., 1995. Photoacoustic investigation of transport in semiconductors: theoretical and experimental study of a Ge single crystal. Phys. Rev. B 51, 14226–14232. http://dx.doi.org/10.1103/PhysRevB.51.14226.
Dupré, O., 2015. Physics of the Thermal Behavior of Photovoltaic Devices Ph.D. thesis. INSA Lyon, France.
Dupré, O., Vaillon, R., 2014. Optimizations of photovoltaic cells including the minimization of internal heat sources. J. Renew. Sustain. Energy 6, 11201. http://dx.doi.org/10.1063/1.4828367.
Dupré, O., Vaillon, R., Green, M.A., 2015. Physics of the temperature coefficients of solar cells. Sol. Energy Mater. Sol. Cells 140, 92–100. http://dx.doi.org/10.1016/j.solmat.2015.03.025.
Francoeur, M., Pinar Mengüç, M., Vaillon, R., 2009. Solution of near-field thermal radiation in one-dimensional layered media using dyadic Green's functions and the scattering matrix method. J. Quant. Spectrosc. Radiat. Transf. 110, 2002–2018. http://dx.doi.org/10.1016/j.jqsrt.2009.05.010.
Francoeur, M., Vaillon, R., Mengüç, M.P., 2011. Thermal impacts on the performance of nanoscale-gap thermophotovoltaic power generators. IEEE Trans. Energy Convers. 26, 686–698. http://dx.doi.org/10.1109/TEC.2011.2118212.
Green, M.A., 1982. Solar Cells: Operating Principles, Technology, and System Applications. Prentice-Hall, Englewood Cliffs, NJ.
Green, M.A., 2012. Radiative efficiency of state of the art photovoltaic cells. Prog. Photovolt. Res. Appl. 20, 472–476. http://dx.doi.org/10.1002/pip.
Harder, N., Green, M.A., 2003. Thermophoton. Semicond. Sci. Technol. 18, S270–S278.
Harder, N., Würfel, P., 2003. Theoretical limits of thermophotovoltaic solar energy conversion. Semicond. Sci. Technol. 151, S151–S157. http://dx.doi.org/10.1088/0268-1242/18/5/303.
Hirst, L.C., Ekins-Daukes, N.J., 2011. Fundamental losses in solar cells. Prog. Photovolt. Res. Appl. 19, 286–293. http://dx.doi.org/10.1002/pip.1024.
Kittel, C., 1996. Introduction to Solid State Physics. John Wiley & Sons Inc.
Koehl, M., Heck, M., Wiesmeier, S., Wirth, J., 2011. Modeling of the nominal operating cell temperature based on outdoor weathering. Sol. Energy Mater. Sol. Cells 95, 1638–1646. http://dx.doi.org/10.1016/j.solmat.2011.01.020.
Kurtz, S., Whitfield, K., Tamizhmani, G., et al., 2011. Evaluation of high-temperature exposure of photovoltaic modules. Prog. Photovolt. Res. Appl. 954–965. http://dx.doi.org/10.1002/pip.
Landsberg, P.T., Badescu, V., 2000. Carnot factor in solar cell efficiencies. J. Phys. D Appl. Phys. 33, 3004–3008. http://dx.doi.org/10.1088/0022-3727/33/22/320.
Mulet, J.-P., Joulain, K., Carminati, R., Greffet, J.-J., 2002. Enhanced radiative heat transfer at nanometric distances. Microscale Thermophys. Eng. 6, 209–222. http://dx.doi.org/10.1080/10893950290053321.
Pipe, K., Ram, R., Shakouri, a., 2002. Bias-dependent Peltier coefficient and internal cooling in bipolar devices. Phys. Rev. B 66, 1–11. http://dx.doi.org/10.1103/PhysRevB.66.125316.
Rau, U., 2007. Reciprocity relation between photovoltaic quantum efficiency and electroluminescent emission of solar cells. Phys. Rev. B 76, 1–8. http://dx.doi.org/10.1103/PhysRevB.76.085303.
Richter, A., Hermle, M., Glunz, S.W., 2013. Reassessment of the limiting efficiency for crystalline silicon solar cells. IEEE J. Photovolt. 3, 1184–1191.
Ross, R., Gonzalez, C., 1980. Reference conditions for reporting terrestrial photovoltaic performance. In: AS/ISES Annual Meeting. pp 1091–1097.
Ross, R.G., Smokler, M.I., 1986. Electricity from photovoltaic solar cells: Flat-Plate Solar Array Project final report. Volume VI: Engineering sciences and reliability.
Skoplaki, E., Palyvos, J.A., 2009a. Operating temperature of photovoltaic modules: a survey of pertinent correlations. Renew. Energy 34, 23–29. http://dx.doi.org/10.1016/j.renene.2008.04.009.
Skoplaki, E., Palyvos, J.A., 2009b. On the temperature dependence of photovoltaic module electrical performance: a review of efficiency/power correlations. Sol. Energy 83, 614–624. http://dx.doi.org/10.1016/j.solener.2008.10.008.
Swanson, R.M., 1979. A proposed thermophotovoltaic solar energy conversion system. Proc. IEEE 67, 446–447. http://dx.doi.org/10.1109/PROC.1979.11270.
Virtuani, A., Pavanello, D., Friesen, G., 2010. Overview of temperature coefficients of different thin film photovoltaic technologies. In: 25th European Photovoltaic Solar Energy Conference and Exhibition/5th World Conference on Photovoltaic Energy Conversion.
Whale, M.D., Cravalho, E.G., 2002. Modeling and performance of microscale thermophotovoltaic energy conversion devices. IEEE Trans. Energy Convers. 17, 130–142. http://dx.doi.org/10.1109/60.986450.
Würfel, P., 2009. Physics of Solar Cells: From Basic Principles to Advanced Concepts. Wiley.